Generalized Differential Morphological Profiles for Remote Sensing Image Classification

Xin Huang, *Senior Member, IEEE*, Xiaopeng Han, Liangpei Zhang, *Senior Member, IEEE*, Jianya Gong, Wenzhi Liao, *Member, IEEE*, and Jon Atli Benediktsson, *Fellow, IEEE*

***Abstract*—Differential morphological profiles (DMPs) are widely used for the spatial/structural feature extraction and classification of remote sensing images. They can be regarded as the shape spectrum, depicting the response of the image structures related to different scales and sizes of the structural elements (SEs). DMPs are defined as the difference of morphological profiles (MPs) between consecutive scales. However, traditional DMPs can ignore discriminative information for features that are across the scales in the profiles. To solve this problem, we propose scale-span differential profiles, i.e., generalized DMPs (GDMPs), to obtain the entire differential profiles. GDMPs can describe the complete shape spectrum and measure the difference between arbitrary scales, which is more appropriate for representing the multiscale characteristics and complex landscapes of remote sensing image scenes. Subsequently, the random forest (RF) classifier is applied to interpret GDMPs considering its robustness for high-dimensional data and ability of evaluating the importance of variables. Meanwhile, the RF "out-of-bag" error can be used to quantify the importance of each channel of GDMPs and select the most discriminative information in the entire profiles. Experiments conducted on three well-known hyperspectral data sets as well as an additional WorldView-2 data are used to validate the effectiveness of GDMPs compared to the traditional DMPs. The results are promising as GDMPs can significantly outperform the traditional one, as it is capable of adequately exploring the multiscale morphological information.**

***Index Terms*—Classification, feature extraction, feature selection, morphological profiles (MPs), random forest (RF).**

I. Introduction

ADVANCES in Earth observation technology, leading to an increased availability of data from different sensors, have opened up new avenues for geospatial information extraction. Recently, remote sensing data can provide wealthy information in spatial domains. However, higher spatial resolution does not naturally correspond to higher image interpretation accuracies, and their availability poses challenges to land cover and land use mapping, especially in urban areas. Due to the complex spatial arrangement and spectral heterogeneity even within the same class, conventional spectral-based classification suffers from a large number of misclassifications between spectrally similar classes [1]. Moreover, submeter resolution images are subject to increase of the intraclass variance and decrease of the interclass variance in the spectral feature space, leading to decreased class separability in the spectral domain [2]. Therefore, there is an increased interest and demand in incorporating geometrical information into the image classification. Specifically, in recent years, a few studies on spectral–spatial joint feature extraction and classification have been proposed. One of the state-of-the-art procedures for spatial feature is the gray-level cooccurrence matrix (GLCM) [3], which is a widely used texture and pattern recognition technique in the analysis of remote sensing data. For instance, recently, a GLCM based on the sparse coding was proposed for hyperspectral texture representation and achieved higher classification accuracy compared to the original GLCM

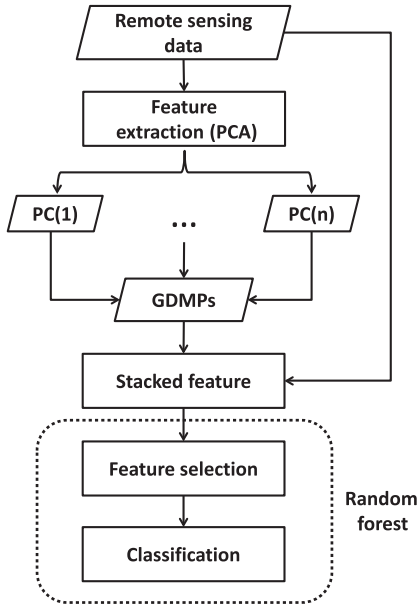

Fig. 1. General workflow of this study.

Manuscript received September 22, 2015; revised December 16, 2015; accepted January 28, 2016. Date of publication February 24, 2016; date of current version March 11, 2016. This work was supported in part by the National Natural Science Foundation of China under Grant 91338111, in part by the China National Science Fund for Excellent Young Scholars under Grant 41522110, and in part by the Foundation for the Author of National Excellent Doctoral Dissertation of China (FANEDD) under Grant 201348. *(Corresponding author: Xin Huang.)*

X. Huang and J. Gong are with the School of Remote Sensing and Information Engineering, and State Key Laboratory of Information Engineering in Surveying, Mapping, and Remote Sensing, Wuhan University, Wuhan 430079, China (e-mail: huang_whu@163.com).

X. Han and L. Zhang are with the State Key Laboratory of Information Engineering in Surveying, Mapping, and Remote Sensing, Wuhan University, Wuhan 430079, China.

W. Liao is with the Department of Telecommunications and Information Processing, Ghent University, Ghent 9000, Belgium.

J. A. Benediktsson is with the Faculty of Electrical and Computer Engineering, University of Iceland, Reykjavik 101, Iceland.

Color versions of one or more of the figures in this paper are available online at http://ieeexplore.ieee.org.

Digital Object Identifier 10.1109/JSTARS.2016.2524586

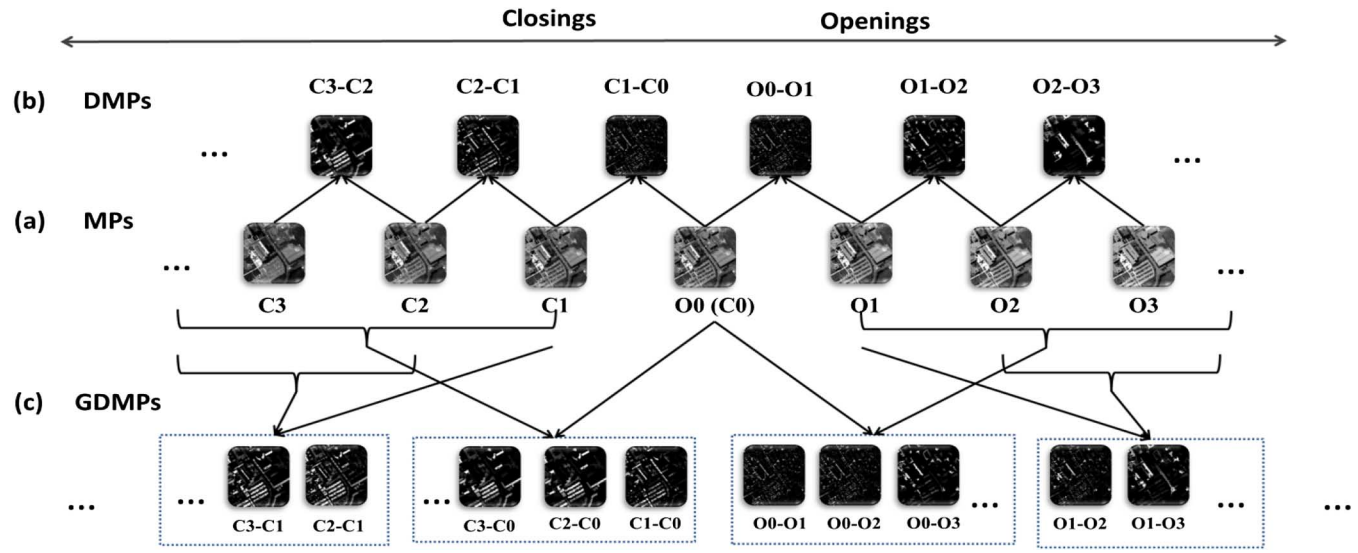

Fig. 2. Demonstrations for: (a) MPs; (b) DMPs; and (c) GDMPs.

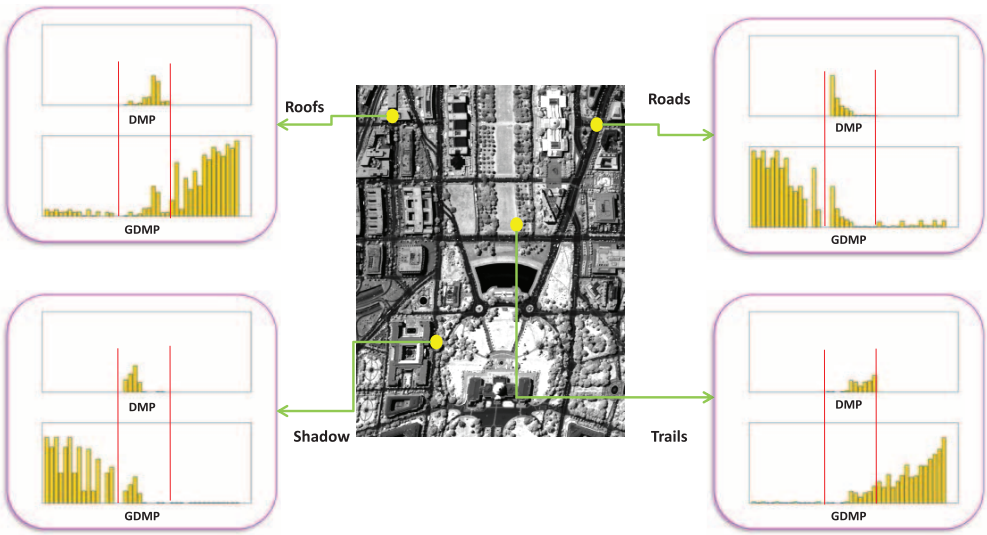

Fig. 3. Comparison between DMPs and GDMPs for several typical information classes (roofs, roads, trails, and shadow). The same profiles for DMPs and GDMPs are noted. The sizes of disk-shaped SEs used in this test vary from 2 to 12 with an interval of two pixels.

[4]. The Markov random-field is also an effective way to take into account spatial information for image interpretation [5]. Other commonly used spatial features include Wavelet transform (WT) [6], pixel shape index (PSI) [7], local binary pattern (LBP) [8]–[10], Gabor filter banks (Gabor) [11], [12], etc., aiming to explore the spatial correlation and structural information for enhancing the traditional spectral-based image classification.

Recently, mathematical morphology, which can effectively explore the spatial and structural information from the remote sensing data, has received more and more attention. In [13], differential morphological profiles (DMPs) were proposed and applied to remote sensing image segmentation and classification. In particular, the segmentation map was obtained by associating each pixel to the level where the DMP value of corresponding pixel reaches the maximum. In [14], dimensionality reduction, e.g., feature extraction and feature selection were applied to the DMPs, and the dimensionally reduced profiles were then fed into a neural network classifier for image classification. DMPs were further investigated in [15], where they were interpreted in terms of a fuzzy measurement of the characteristic size and contrast of each structure. The fuzzy measure was compared to a set of predefined possibility distributions to derive a membership degree for various land cover classes. Morphological texture features were applied to mangrove forest mapping and species discrimination in [16]. MPs can be extended for representing image structures for hyperspectral images [17], where MPs are computed on the first few principal components (PCs) of hyperspectral data, called extended morphological profiles (EMPs). More recently, morphological attribute profiles (APs) were proposed, providing a variety of attributes (e.g., area, volume, moment of inertia) based on a multilevel characterization of an image using connected operators [18]. In [19] and [20], extended APs (EAPs) were presented by calculating the APs on the independent components of hyperspectral data. Furthermore, a set

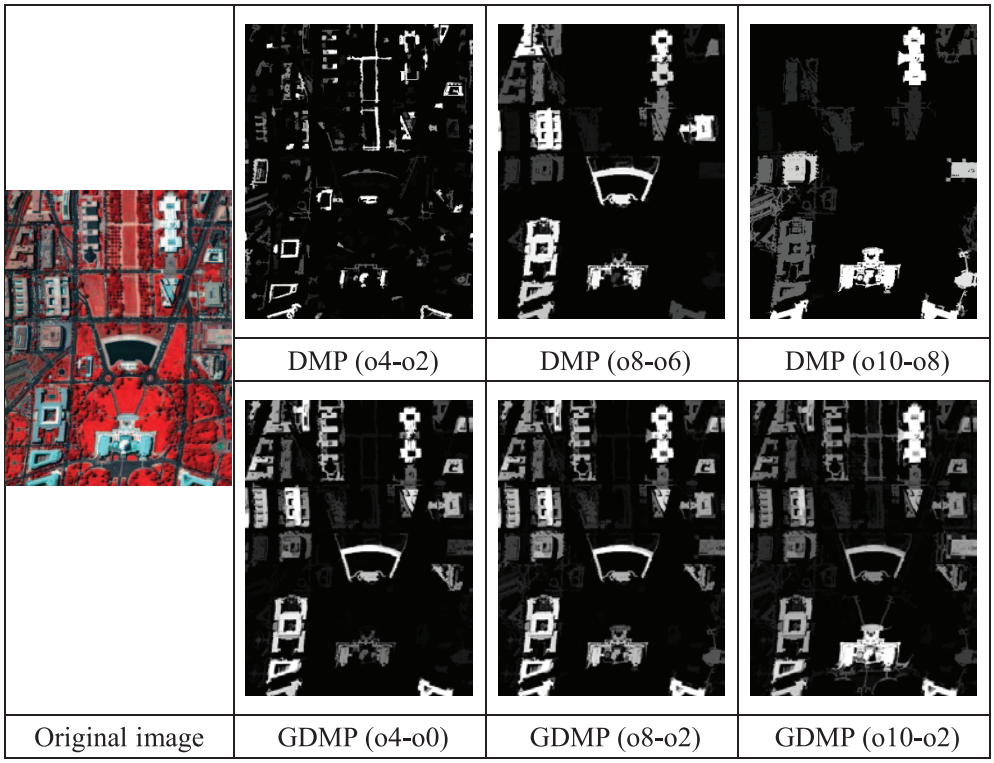

Fig. 4. Comparison for pattern representation of buildings between DMPs and GDMPs. The sizes of disk-shaped SEs used in this test vary from 2 to 12 with an interval of two pixels. For instance, the symbol "o4-o2" means the difference of opening-by-reconstruction between scale 4 and scale 2.

of new multiple morphological profiles (MMPs) were created by integrating the MPs derived from multiple base images produced by various strategies, including linear, nonlinear, multilinear image transformation, and manifold learning methods [21]. A survey on the spectral–spatial classification techniques based on morphological profiles (MPs) can be found in [22].

Among these MPs, DMPs, regarded as the shape spectrum of objects, have been proved effective in describing the structural and spatial features from remote sensing images and achieved promising performances. DMPs are constructed on the repeated use of openings and closings by a series of structuring element (SE) with increasing sizes. However, DMPs focus on the differences between consecutive scales with a constant interval, which actually ignore the across-scale information (i.e., the difference between any two scales) in the MPs and lead to underutilization of the discriminative features. In this regard, therefore, the objective of the proposed generalized DMPs (GDMPs) is to describe the entire shape spectrums and measure the difference between two arbitrary scales with a variable interval from the MPs.

This paper is organized as follows. Section II briefly introduces the principles of GDMPs using geodesic and partial reconstruction, respectively, followed by introduction of RF classifier for GDMPs feature selection and classification. Experimental results and the corresponding analysis are presented in Section III, and Section IV concludes this study with some remarks and hints at plausible future research.

II. Methodology

Erosion and dilation are the basic operators of grayscale mathematical morphology [28]. The operators are applied to an image with a set of known shapes (e.g., disk, square), called SEs. Erosion and dilation can be used to define the commonly used morphological operators: opening and closing. Morphological opening is to dilate an eroded image aiming at isolating bright structures, and closing is to erode a dilated image for suppressing dark structures. In order to preserve the shape of the objects and introduce less shape noise, geodesic reconstruction [25], [13]–[15], and partial reconstruction [26] are used. The proposed GDMPs are defined on the basis of the aforementioned grayscale morphological processing. The processing chain of the GDMPs is shown in Fig. 1. Note that in this study, in order to adequately verify the effectiveness of the GDMPs, both geodesic morphological reconstruction [13]–[15], [25] and partial morphological reconstruction [26], [27] are employed for constructing the GDMPs. Furthermore, considering the high-dimensional feature space and redundant information caused by GDMPs, in this study, random forest (RF) is employed for interpreting GDMPs, i.e., in classification. The importance of each element in the entire profiles can be quantified by using the "out-of-bag" analysis [23], [24]. In this way, the feature selection is performed and larger weights are given to the more discriminative features in the profiles.

A. GDMPs

MPs [17], [29] are implemented on a series of morphological openings and closings with a family of SEs of increasing sizes. Let $\gamma_\lambda(I)$ and $\phi_\lambda(I)$ be the morphological opening and closing for an image I, respectively, with λ representing the radius of the disk-shaped SE considered in this study. MPs can be defined using a series of SEs with increasing sizes [Fig. 2(a)]

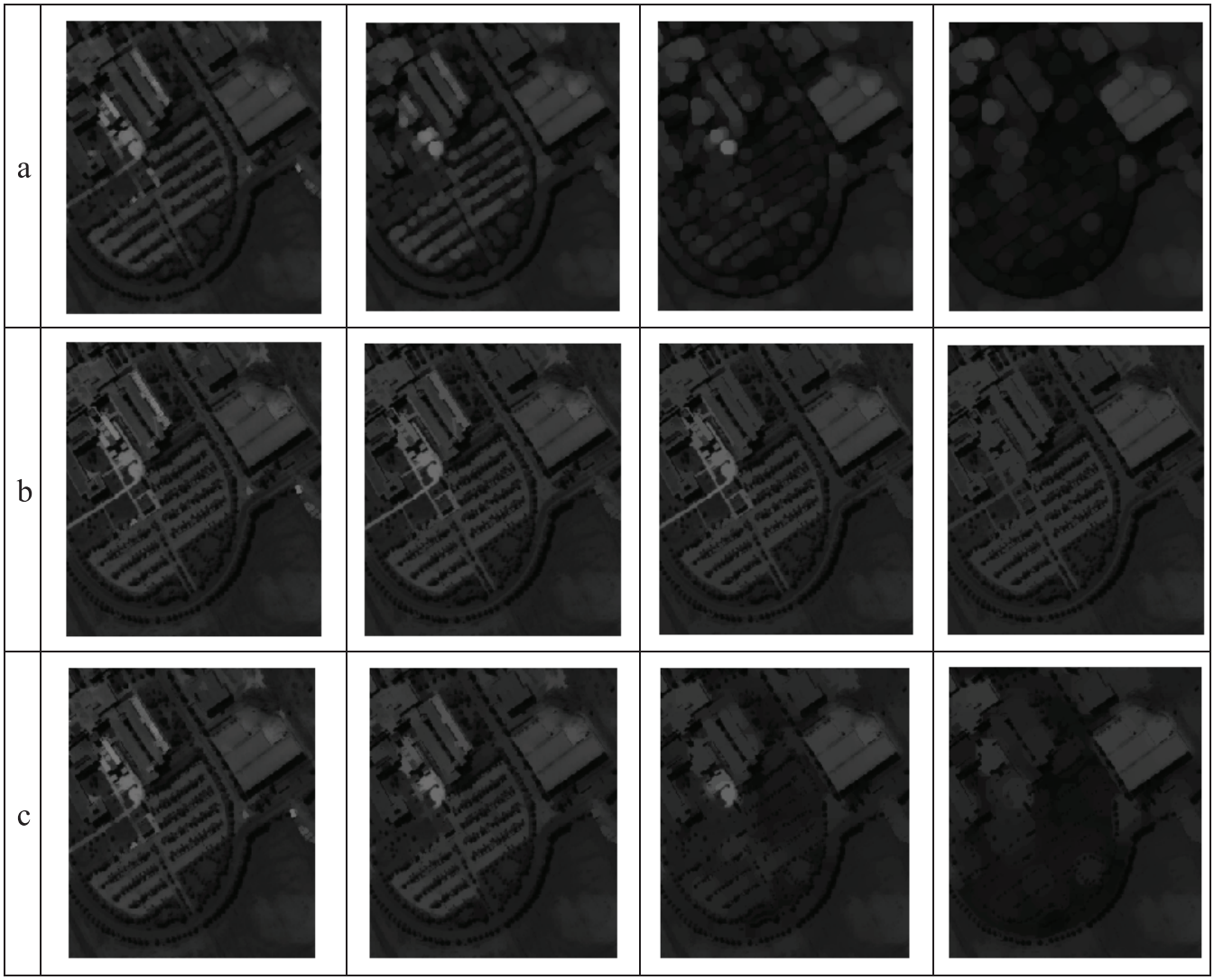

Fig. 5. Demonstration and comparison between different morphological reconstruction methods by using opening with disk-shaped SEs of increasing sizes. The sizes of SE vary from 2 to 8 with an interval of two pixels. The image shown is a subset of the Pavia University image [Fig. 6(b)]: rows 1–3 correspond to without reconstruction, geodesic reconstruction, and partial reconstruction, respectively.

$$MP_\gamma = \{MP_{\gamma_\lambda}(I) = \gamma_\lambda(I), \quad \forall \lambda \in [0, n]\} \tag{1}$$

$$MP_\phi = \{MP_{\phi_\lambda}(I) = \phi_\lambda(I), \quad \forall \lambda \in [0, n]\} \quad with\ \gamma_0(I) = \phi_0(I) = I. \tag{2}$$

Subsequently, DMPs are defined as the differences of MPs between consecutive scales [i.e., λ and $(\lambda - 1)$] [Fig. 2(b)]

$$DMP_\gamma = \{DMP_{\gamma_\lambda}(I) = |MP_{\gamma_{\lambda+1}}(I) - MP_{\gamma_\lambda}(I), \quad \lambda \in [0, n-1]\} \tag{3}$$

$$DMP_\phi = \{DMP_{\phi_\lambda}(I) = |MP_{\phi_{\lambda+1}}(I) - MP_{\phi_\lambda}(I), \quad \lambda \in [0, n-1]\}. \tag{4}$$

In general, DMP_γ and DMP_ϕ are often concatenated into a DMP vector in order to represent both bright and dark objects in an image: $DMP = \{DMP_\gamma, DMP_\phi\}$

Equations (3) and (4) indicate that DMPs are the differences of MPs between consecutive scales with a constant interval. In this way, however, the across-scale information in the MPs is ignored. To obtain scale-span morphological features, GDMPs [see Fig. 2(c)] are proposed and defined as

$$GDMP_\gamma = \{GDMP_{\gamma_\lambda}(I)|MP_{\gamma_{\lambda+i}} - MP_{\gamma_\lambda}, \quad i \in [1, n],\ \lambda \in [0, n-i]\} \tag{5}$$

$$GDMP_\phi = \{GDMP_{\phi_\lambda}(I)|MP_{\phi_{\lambda+i}} - MP_{\phi_\lambda}, \quad i \in [1, n],\ \lambda \in [0, n-i]\}. \tag{6}$$

GDMPs are created on all possible scale intervals in the MPs. Similarly, $GDMP_\gamma$ and $GDMP_\phi$ are then concatenated into a GDMP vector for classification: $GDMP = \{GDMP_\gamma, GDMP_\phi\}$.

Examples of DMPs and GDMPs for several typical information classes are shown in Fig. 3, where the striking difference between DMPs and GDMPs can be observed. Notably, from Fig. 3, it can be also seen that DMPs are the subset of GDMPs, and the latter can provide more discriminative information.

In addition, in this study, the objective of GDMPs is to further enhance the ability of the traditional DMPs for scale and

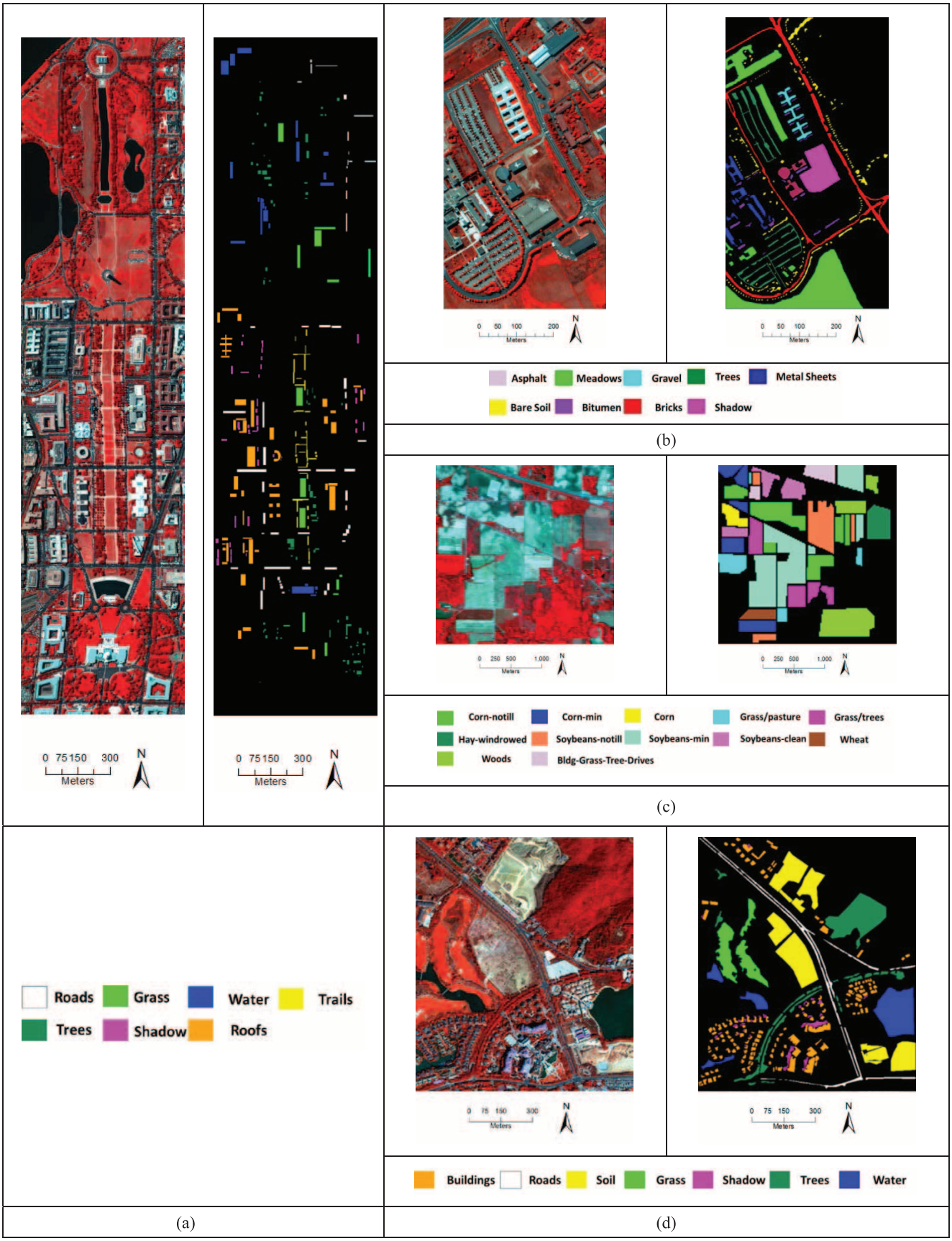

Fig. 6. Test data sets and their reference maps. (a) HYDICE DC Mall. (b) ROSIS Pavia University. (c) AVIRIS Indian pines. (d) Worldview-2 Hainan.

TABLE I
NUMBER OF TRAINING AND TEST SAMPLES (HYDICE DC MALL)

Information classes	No. of test samples
Roads	3334
Grass	3075
Water	2882
Trails	1034
Trees	2047
Shadow	1093
Roofs	5867
Total	19 332

TABLE II
NUMBER OF TRAINING AND TEST SAMPLES (PAVIA UNIVERSITY)

Information classes	No. of test samples
Asphalt	6631
Meadows	18 649
Gravel	2099
Trees	3064
Metal sheets	1345
Bare soil	5029
Bitumen	1330
Bricks	3682
Shadow	947
Total	42 776

TABLE III
NUMBER OF TRAINING AND TEST SAMPLES (INDIAN PINES)

Information classes	No. of test samples
Corn-notill	1434
Corn-min	834
Corn	234
Grass/pasture	497
Grass/trees	747
Hay-windrowed	489
Soybeans-notill	968
Soybeans-min	2468
Soybeans-clean	614
Wheat	212
Woods	1294
Bldg-grass-tree-drives	380
Total	10 171

pattern representation, by considering the scale-span differential profiles. An interesting example is demonstrated in Fig. 4. Comparing the results between DMPs and GDMPs, it can be clearly seen that the objects (in this case, the buildings) were divided into several parts, corresponding to different scales of the DMPs. However, by courtesy of the across-scale representation, GDMPs can describe the buildings more completely.

B. Partial Reconstruction of GDMPs

When using geodesic reconstruction, the whole objects can be reconstructed if at least one pixel of the object survives the opening or closing. However, MPs with geodesic reconstruction may lead to over-reconstruction, i.e., some objects that disappeared in the MP without reconstruction may remain present in the MP with geodesic reconstruction. As shown in Fig. 5(a), the small bright roads on the middle left disappear at a certain scale (SE = 6), but these roads still exist when the size of SE reaches 6 in Fig. 5(b). To solve this problem, partial reconstruction [26] was introduced. If a pixel is connected

TABLE IV
NUMBER OF TRAINING AND TEST SAMPLES (WORLDVIEW-2 HAINAN)

Information classes	No. of test samples
Buildings	11 578
Roads	5357
Soil	22 189
Grass	7417
Shadow	1427
Trees	14 086
Water	11 209
Total	73 263

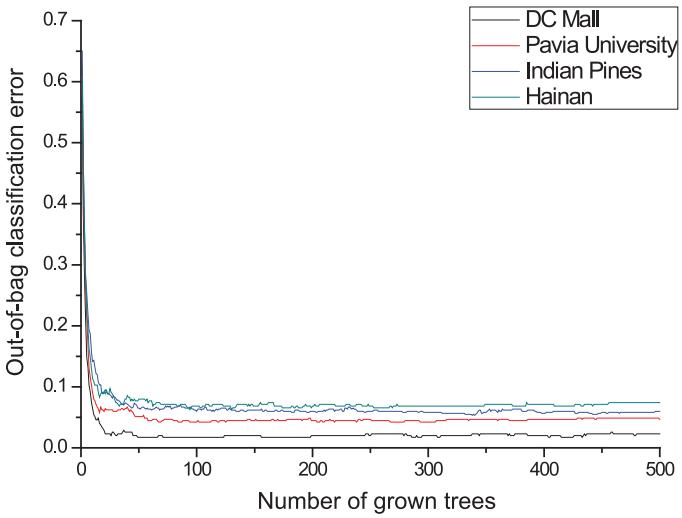

Fig. 7. Relationship between "out-of-bag" classification error and the number of decision trees of RF. It can be observed that after 100–200 trees used in the forest, classification accuracies become steady.

TABLE V
ACCURACIES (%) FOR DMPS AND GDMPS WITH GEODESIC RECONSTRUCTION FOR THE DC MALL IMAGE

	Feature		
Classes	RAW	DMPs	GDMPs
Roads	97.97±1.89	97.88±1.73	98.00±1.32
Grass	99.54±0.89	99.84±0.84	100.00±0.71
Water	99.51±1.65	99.72±1.36	100.00±0.07
Trails	95.38±1.64	97.05±1.95	98.82±2.50
Trees	98.42±0.46	98.42±0.49	98.67±0.38
Shadow	98.26±1.21	98.63±0.99	98.90±0.37
Roofs	79.28±4.29	81.05±3.92	93.44±3.85
OA	92.73±1.22	93.43±1.12	97.41±1.21
AA	95.48±0.49	96.08±0.45	98.26±0.58
Kappa	91.18±1.47	92.03±1.35	96.82±1.47

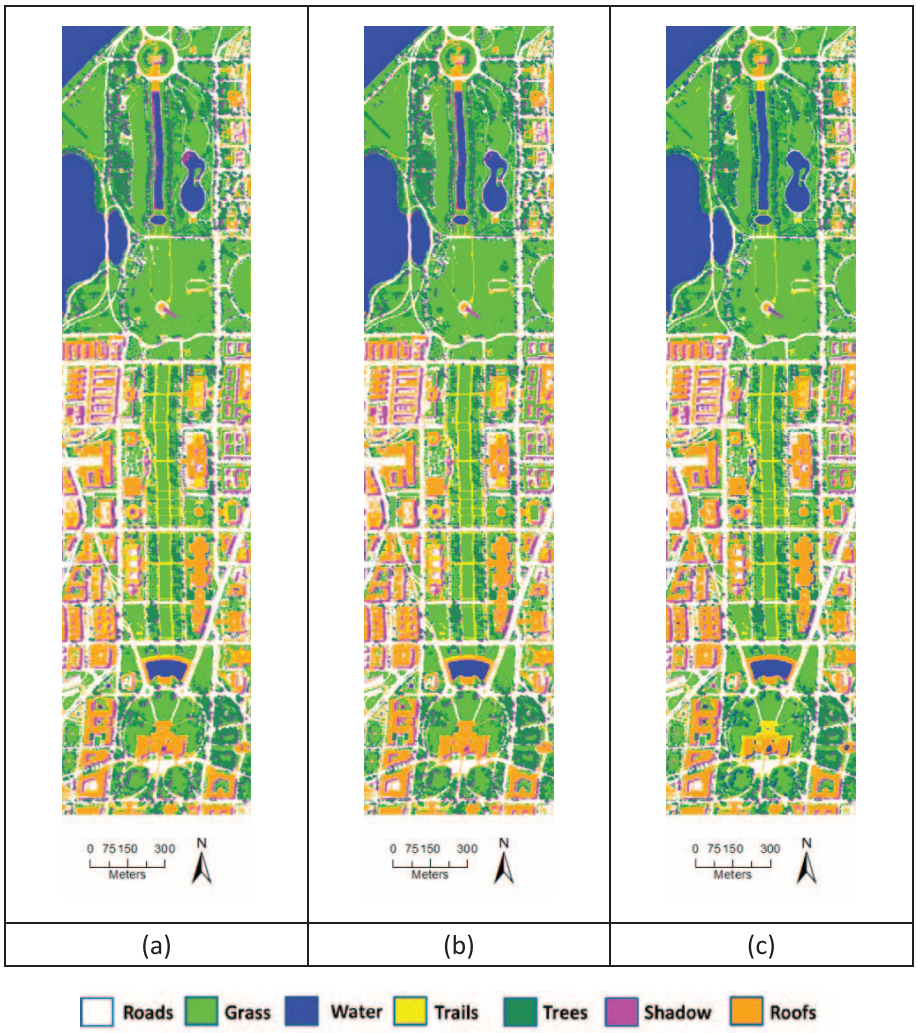

Fig. 8. RF classification maps for the DC Mall image. (a) Raw hyperspectral image. (b) DMPs. (c) GDMPs.

TABLE VI
ACCURACIES (%) FOR DMPS AND GDMPS WITH GEODESIC RECONSTRUCTION FOR THE PAVIA UNIVERSITY IMAGE

	Feature		
Classes	RAW	DMPs	GDMPs
Asphalt	72.22±2.32	96.52±2.08	98.36±2.19
Meadows	67.92±5.35	77.39±5.41	95.10±4.11
Gravel	65.22±5.46	89.14±4.27	96.24±1.10
Trees	86.65±3.55	95.43±2.79	95.82±1.67
Metal sheets	98.74±0.29	99.11±0.28	98.88±0.21
Bare soil	76.38±4.65	89.14±3.56	94.55±3.23
Bitumen	89.70±2.19	98.05±0.59	94.51±1.17
Bricks	76.15±4.86	85.12±5.37	97.18±1.25
Shadow	100.00±0.00	100.00±0.00	100.00±0.00
OA	73.85±2.14	86.62±2.40	96.22±1.67
AA	81.44±0.81	92.18±1.02	96.98±0.57
Kappa	67.03±2.32	82.87±2.92	95.28±2.09

to another pixel that was not removed after opening or closing and the distance between two connected pixels is smaller than a certain value, the pixel is reconstructed. It should be noted that the geodesic distance, which refers to the length of the shortest path between the two pixels that lies entirely within the object, is used to measure the distance between the two connected pixels and determine the amount of reconstruction. As shown in Fig. 5(c), MPs with partial reconstruction overcomes the problem of over-reconstruction while preserving the shape of objects as much as possible.

The GDMPs with partial reconstruction can be similarly expressed using (5) and (6). Their performance will also be evaluated by the data sets in this study.

C. Feature Selection of GDMPs

Since the proposed GDMPs depict the entire DMPs, they necessarily contain a lot of redundancies in the feature space. Therefore, RFs are used in this research to select the most relevant features from GDMPs. RF are a combination of bagging classification trees that have demonstrated an excellent performance in terms of classification accuracies among a variety of machine learning algorithms [23], [24]. Each classification tree of RF is grown using a bootstrapped sample from the original training samples. At each node of the tree, a series of

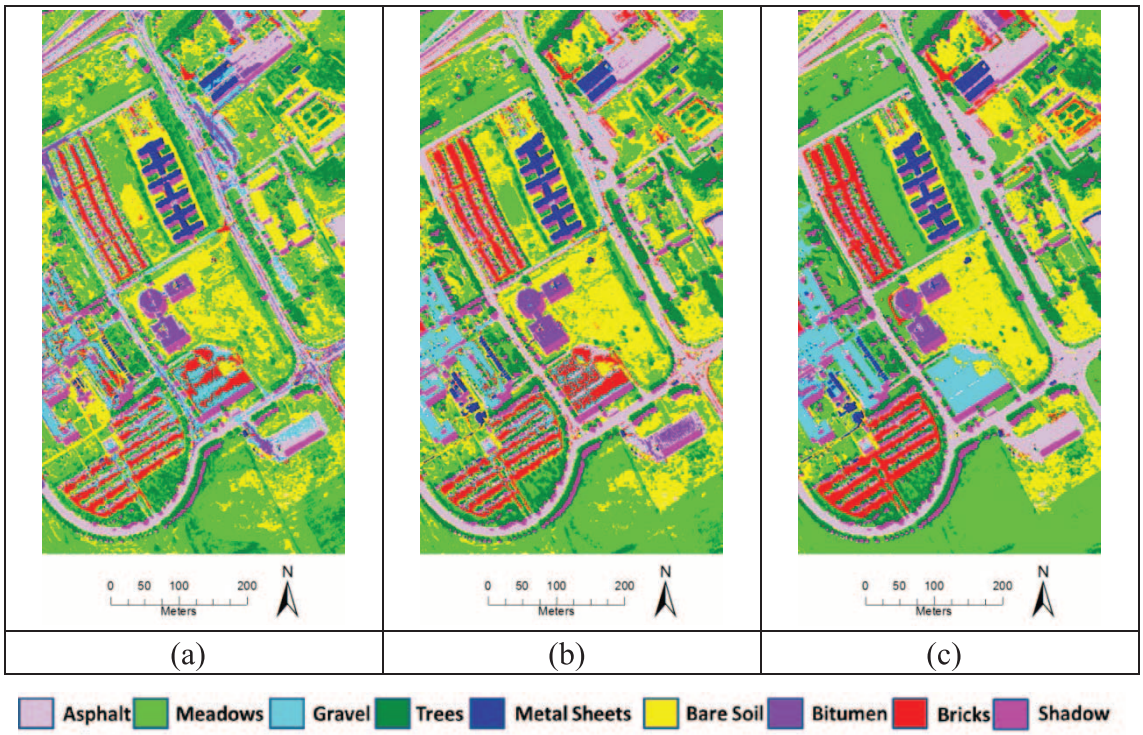

Fig. 9. Classification maps for the Pavia University image. (a) Raw hyperspectral image. (b) DMPs. (c) GDMPs.

TABLE VII
ACCURACIES (%) FOR DMPS AND GDMPS WITH GEODESIC RECONSTRUCTION FOR THE INDIAN PINES IMAGE

Feature			
Classes	RAW	DMPs	GDMPs
Corn-notill	58.30±3.82	74.41±3.09	81.80±2.52
Corn-min	56.47±3.91	84.77±4.06	95.32±3.11
Corn	78.21±6.18	90.60±2.36	98.29±1.73
Grass/pasture	86.12±3.34	88.73±2.79	90.14±2.49
Grass/trees	91.03±5.07	97.59±2.84	99.38±2.67
Hay-windrowed	98.36±0.54	98.77±0.44	99.18±0.46
Soybeans-notill	79.44±4.01	84.81±3.66	85.12±2.59
Soybeans-min	55.79±6.52	90.40±3.08	96.43±2.89
Soybeans-clean	63.86±3.80	89.58±2.23	90.72±3.69
Wheat	98.11±2.57	98.58±1.65	99.06±1.56
Woods	86.17±4.11	92.19±1.80	96.06±0.57
Bldg-grass-tree-drives	58.95±3.26	95.00±2.72	96.84±1.17
OA	70.43±1.88	88.53±1.05	92.45±0.73
AA	75.89±1.01	90.45±0.77	93.89±0.39
Kappa	66.80±2.01	86.94±1.19	91.43±0.83

independent variables are randomly selected, decreasing the correlation between the trees in the forest. When choosing the best split from the selected variables at each node, the Gini index [30], [31] indicating the impurity with the lowest value is used to select the most important feature. Subsequently, the most important feature is used to split the corresponding node. Let T represent training set and C_i represent a certain information class, Gini index can be written as

$$\sum \sum_{j \neq i} (f(C_i, T)/|T|)(f(C_j, T)/|T|) \tag{7}$$

where $f(C_i, T)/|T|$ is the probability that the selected pixel belongs to class C_i.

Each time, a tree is grown into a maximally sized tree without pruning or stopping rules, forming a combination of tree classifier, namely RF. Since each tree of RF is grown from a bootstrapped sample, in general, about one-third of the observed training samples will not be used when growing a tree. These observations are called "out-of-bag" samples, forming a natural test for each tree. Variable importance is represented by the decrease in accuracy using "out-of-bag" observations when permuting the values of the corresponding variables. Compared with other machine learning algorithms, RF not only has a good performance for classification but also provides insight regarding the discriminative ability of each attribute, which actually facilitate to understand the performance of GDMPs. In addition, RF can handle high-dimensional feature space with less computation and be insensitive to noise in training samples [32], [33].

III. EXPERIMENTS

A. Data Sets

The proposed GDMPs are validated on four widely used and public remote sensing data sets: hyperspectral digital-imagery collection experiment (HYDICE) DC Mall, reflective optics system imaging spectrometer (ROSIS) Pavia University, airborne visible/infrared imaging spectrometer (AVIRIS) Indian pines, and Worldview-2 Hainan, respectively. The four data sets are discussed in details below.

1) DC data set was collected by HYDICE sensor in August 1995 over the Washington, DC Mall. This data set

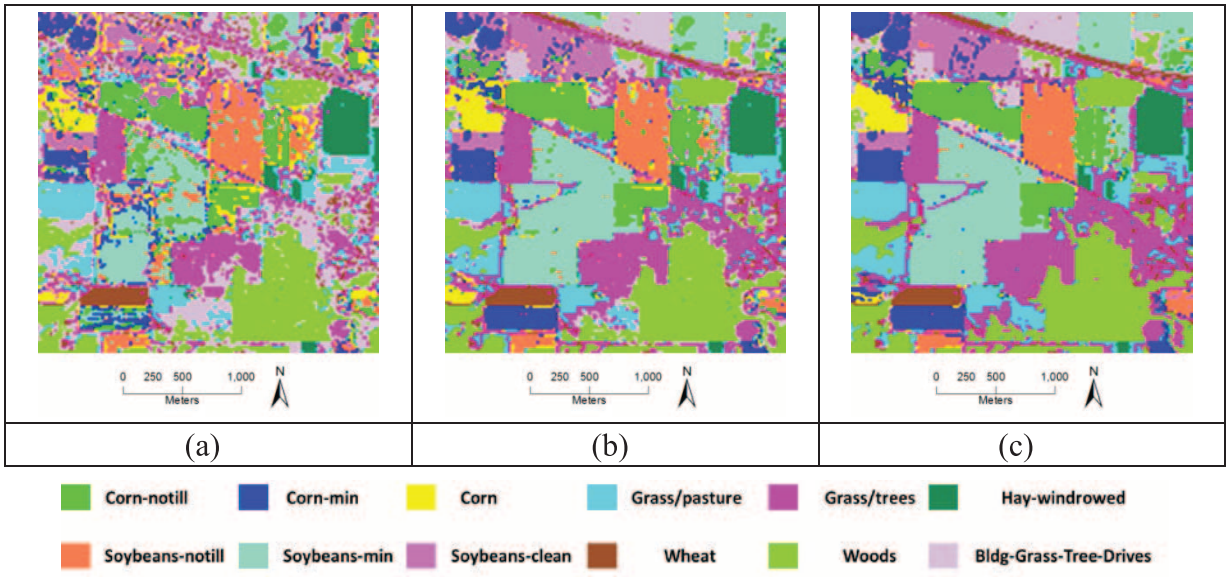

Fig. 10. Classification maps for the Indian Pines image. (a) Raw hyperspectral image. (b) DMPs. (c) GDMPs.

TABLE VIII
ACCURACIES (%) OF DMPS AND GDMPS WITH GEODESIC RECONSTRUCTION FOR THE HAINAN IMAGE

	Feature		
Classes	RAW	DMPs	GDMPs
Buildings	58.31±2.14	86.04±3.70	92.82±2.45
Roads	84.60±2.59	93.84±2.63	96.98±3.04
Soil	91.06±2.40	98.10±1.37	98.74±1.47
Grass	96.85±1.38	98.10±0.73	98.76±0.31
Shadow	91.10±2.47	92.29±2.05	94.86±2.26
Trees	89.73±2.48	92.30±2.13	92.84±2.07
Water	99.80±0.27	99.80±0.14	99.90±0.03
OA	87.08±0.92	94.31±0.99	96.59±0.69
AA	87.35±0.32	94.14±0.68	96.41±0.54
Kappa	84.07±1.11	93.28±1.23	95.98±0.85

originally contained 210 bands within the range of wavelength between 0.4 and 2.4 μm. Noisy channels due to water absorption were removed, resulting in 191 spectral channels available. The main characteristic of DC data set is that it covers an urban area, showing high resolution in both spectral and spatial domains (191 spectral bands with 2.5-m spatial resolution). Spectral characteristics for the same information class are complex (e.g., roofs in the scene are constructed by different materials). However, spectral characteristics of different land cover classes (trees-grass, roofs-trails-roads, water-shadow) are similar due to their overlapped spectral reflectance, making the classification a challenging task. As shown in Fig. 6(a), this image consists of 1280×307 pixels, with 19 332 pixels labeled as a reference for algorithm verification (Table I).

2) The second data set was acquired over the Engineering School at the University of Pavia by the ROSIS sensor. This data set originally contained 115 spectral bands with wavelength ranging from 0.43 to 0.86 μm, with 1.3-m spatial resolution. Some noisy channels have been removed, resulting in 103 spectral bands. This data set also shows an urban landscape, with nine classes of interest. The challenges for this data set refer to: 1) discrimination between trees, meadows, and soil; and 2) discrimination between asphalt, roofs made of different materials (e.g., bitumen, bricks), as the spectral reflectance of these land cover classes are quite similar. As shown in Fig. 6(b), this image consists of 610×340 pixels, with 42 776 labeled pixels for model validation (Table II).
3) The third data set was captured over Northwest Indiana by the AVIRIS sensor. This data set consists of 220 spectral bands with a wavelength range from 0.4 to 2.5 μm. The spatial resolution of this data set is 20 m/pixel. This image covers an agriculture area, and the relative low resolution makes the classification difficult due to the presence of highly mixed pixels. In addition, the number of pixels in the reference data for different information classes is significantly different, which also makes the classification more complicated [33]. As shown in Fig. 6(c), this image consists of 145×145 pixels, with 10 171 labeled pixels for model validation (Table III).
4) The last data set is WorldView-2 high spatial resolution (HSR) data with a 2-m spatial resolution and eight multispectral bands, over a suburban area in the Hainan province of China. As shown in Fig. 5(d), this image consists of 600×520 pixels, with 31 399 labeled pixels for testing different algorithms (Table IV).

B. Experimental Setup

The parameter settings in the experiments are listed below.

1) Morphological profiles: Disk-shaped SEs ranging from 2 to 12 are used to obtain DMPs and GDMPs on the first

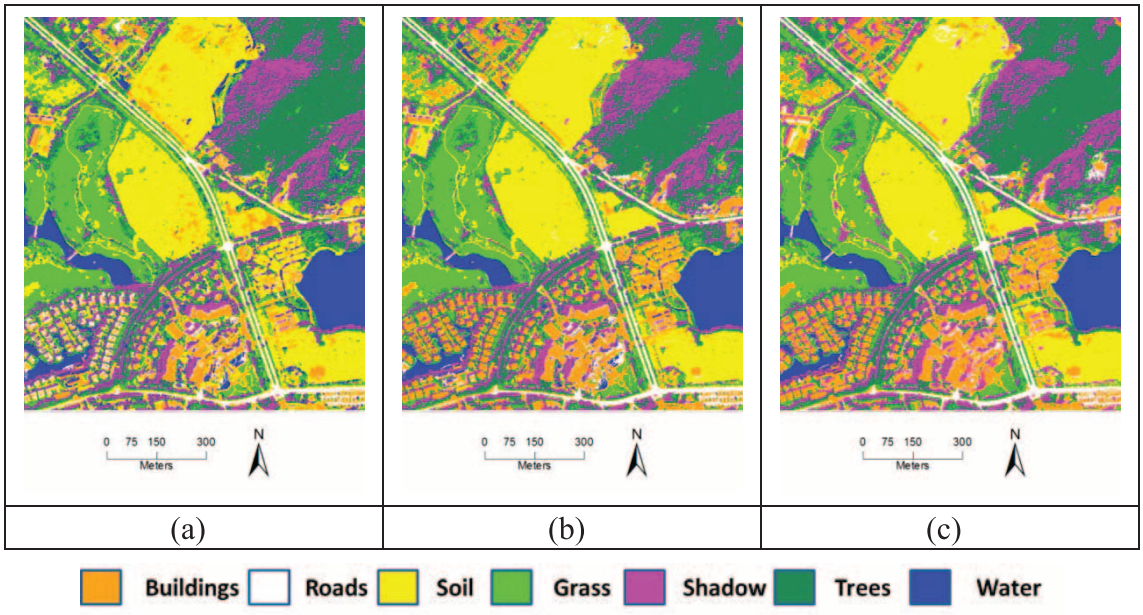

Fig. 11. RF classification maps for the Hainan image: (a) The raw hyperspectral image, (b) DMPs, and (c) GDMPs.

three PCs of original image with geodesic reconstruction and partial reconstruction, respectively.

2) Classifier: RF is used for feature selection and classification with 200 decision trees, by considering both accuracy and efficiency (analyzed in Fig. 7).
3) Accuracy assessment: Overall accuracy (OA), average accuracy (AA), and kappa coefficient (Kappa) computed from the confusion matrix are used to evaluate the classification accuracies.
4) Training: 50 samples per class selected from the reference map are used to train the RF model. The experiments are repeated ten times with different starting training samples and the average accuracies are reported.

C. Experimental Results With Geodesic Reconstruction

Test 1: The class-specific accuracies of the HYDICE DC Mall based on classification of DMPs and GDMPs are presented in Table V. The classification maps of DMPs and GDMPs are shown in Fig. 8. In this data set, the raw spectral-based classification has difficulty in discriminating between roofs, roads, and trails. The classification accuracies can be improved by introducing DMPs and GDMPs. Specifically, compared to the raw classification, the improvements of OA achieved by using DMPs and GDMPs are 0.7% and 4.7%, respectively. For a visual comparison, compared to raw spectral-based classification, the accuracy improvements achieved by DMPs and GDMPs for each class are shown in Fig. 12(a). It can be seen that GDMPs outperform DMPs in terms of the accuracy scores. In particular, GDMPs can improve the accuracies of roofs significantly (from 81% to 93%), which can be attributed to exploitation of the entire shape spectrum considered in the GDMPs.

Test 2: The class-specific accuracies of the Pavia University in classification based on the DMPs and GDMPs are presented in Table VI. The classification maps based on DMPs and GDMPs are shown in Fig. 9. Similarly as in *Test 1*, DMPs and GDMPs can obtain satisfactory results, compared with spectral-based classification (OA is substantially increased from 73.85% to 86.62% and 96.22%, respectively). It can also be seen that the GDMPs surpass DMPs on the classification accuracies significantly as the former considers the entire MPs. In this experiment, the improvements for the class-specific accuracies compared to the raw spectral-based classification are shown in Fig. 12(b). It can be seen that the use of DMPs and GDMPs provides higher accuracies for all the classes. In particular, the increments of the accuracies achieved by the proposed GDMPs are much higher than with the traditional DMPs, especially for the classes meadows, gravel, bare soil, and bricks.

Test 3: The class-specific accuracies of the Indian Pines image achieved by using the DMPs and GDMPs are presented in Table VII. The classification maps for DMPs and GDMPs are compared in Fig. 10 for a visual inspection. For this data set, the original spectral-based classification has difficulty in correctly classifying the 12 information classes, resulting in a relatively low OA (70.43%). However, the OA is significantly raised to 88.53% and 92.45%, respectively, by employing DMPs and GDMPs. The accuracy increment for each class is demonstrated in Fig. 12(c), where a similar phenomenon is observed, i.e., GDMPs are superior to DMPs interms of classification accuracies for most information classes. Please note that this test image is related to an agricultural area, which shows that the proposed GDMPs are not only effective in urban area but also in agricultural areas.

Test 4: The class-specific accuracies of the WorldView-2 Hainan image achieved by using DMPs and GDMPs are provided in Table VIII. Furthermore, their classification maps are shown in Fig. 11. For this data set, the OA of the initial spectral-only classification is 87.08%, subject to the misclassifications between buildings, roads, and soil. The incorporation

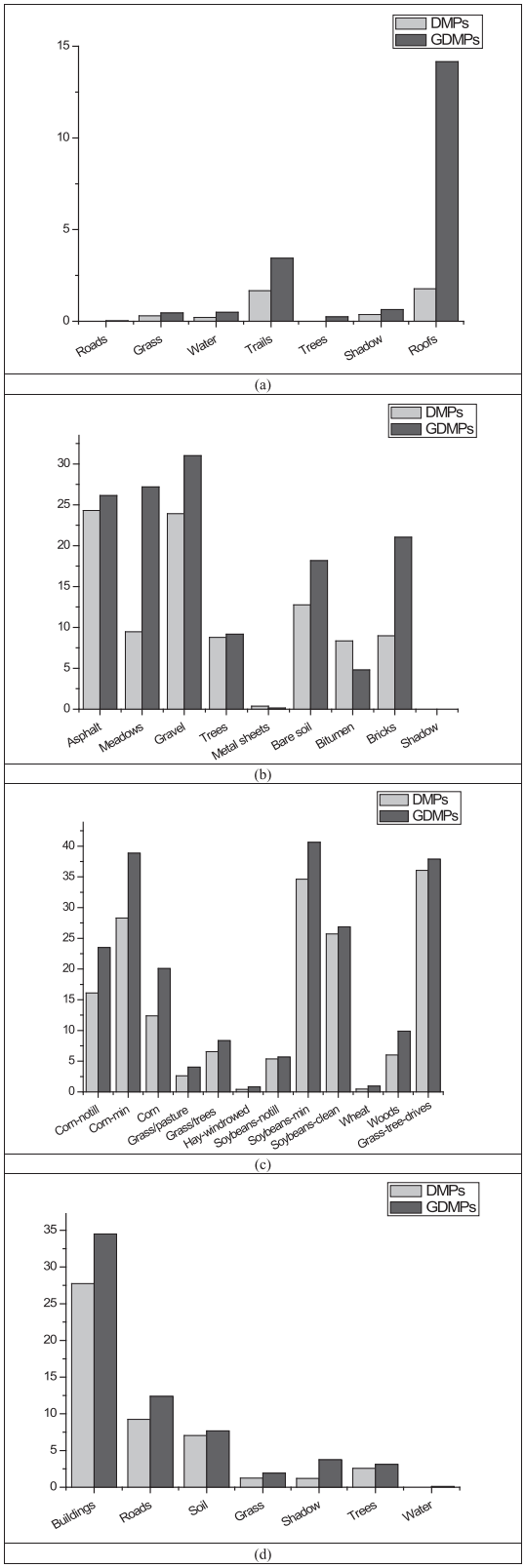

Fig. 12. Percentage of accuracy improvements of each class by the DMPs/GDMPs (geodesic reconstruction) compared to the raw spectral-based method in: (a) DC image; (b) Pavia University; (c) Indian Pines; and (d) Hainan.

of the spatial information can increase the accuracy (OA) by 7.23% and 9.51% for DMPs and GDMPs, respectively. For the improvements of the class-specific accuracy compared to the spectral-based classification [Fig. 12(d)], it can be observed that once again GDMPs provide better results for all the information classes than the traditional DMPs, especially for the buildings (86.04% for the DMPs and 92.82% for the GDMPs), as the proposed GDMPs can describe the structural features in a more appropriate manner.

TABLE IX
COMPARISON OF OA (%) ACHIEVED BY SPECTRAL BANDS, DMPS, AND GDMPS WITH PARTIAL RECONSTRUCTION

Features			
Data sets	RAW	DMPs-partial	GDMPs-partial
DC Mall	92.73	93.85	96.54
Pavia University	73.85	86.16	90.26
Indian Pines	70.43	87.96	91.08
Hainan	87.08	94.94	96.24

D. Experiment Results With Partial Reconstruction

Next, a comparative analysis for DMPs and GDMPs, by partial reconstruction (DMPs-partial, GDMPs-partial), respectively, was conducted. The results are given in Table IX. From the results, it can be observed that GDMPs-partial outperforms the DMPs-partial in all the test data sets. Specifically, compared to the classification accuracy of DMPs-partial, the improvements for GDMPs-partial in OA are about 2.69%, 4.10%, 3.12%, and 1.3% for the DC Mall, Pavia University, Indian Pines, and Hainan data sets, respectively. It is shown that the proposed GDMPs can also provide more accurate classification result under the circumstance of the morphological partial reconstruction.

E. Feature Analysis

In order to analyze the information redundancy of GDMPs and investigate the relationship between classification accuracy (OA) and dimensionality of the feature space, feature selection was conducted according to feature importance quantified by RF *"*out-of-bag*"* error. Fig. 14 shows the relationship between classification accuracy and the dimensionality of the feature space which simultaneously consists of hyperspectral space and GDMPs (geodesic reconstruction). It can be found that curves become stable when dimensionalities of a feature reach a certain number and the turning points of the accuracy curves after which the trend becomes stable are 11, 13, 41, and 45, corresponding to DC Mall, Pavia University, Indian Pines, and Hainan, respectively.

Moreover, a detailed analysis on the source of selected features was conducted.

1) *DC Mall:* The turning point corresponds to 11 features, which can obtain similar classification accuracy with the full feature space [Fig. 14(a)]. Among these 11 selected features, 10 features are derived from GDMPs, and all the 10 features are from the across-scale MPs that cannot be obtained by the traditional DMPs.
2) *Pavia University:* In this test, according to the accuracy curve [Fig. 14(b)], 12 of 13 selected features are from the across-scale DMPs (GDMPs).

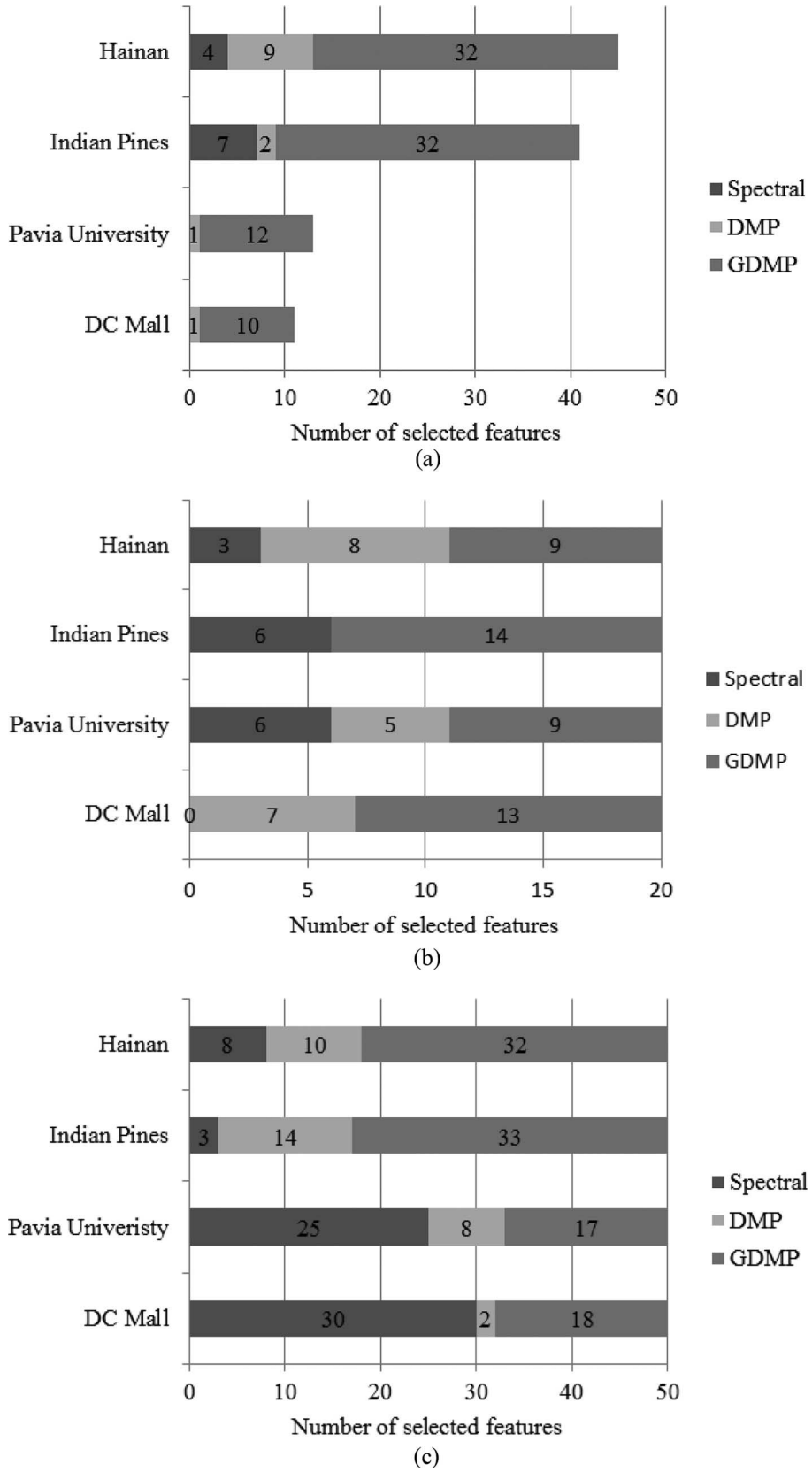

Fig. 13. Feature importance analysis at: (a) turning point; (b) first 20-D; and (c) first 50-D in the hybrid feature space selected.

3) *Indian Pines:* In this case, the first 41 features are selected and analyzed since they can achieve similar classification accuracy with the full feature space [Fig. 14(c)]. However, only 2 of the 41 selected features come from original spectral data, and the remaining 39 features are generated by GDMPs. Please note that 32 of these 39 GDMPs refer to the across-scale MPs, but only 7 features refer to the traditional DMPs.

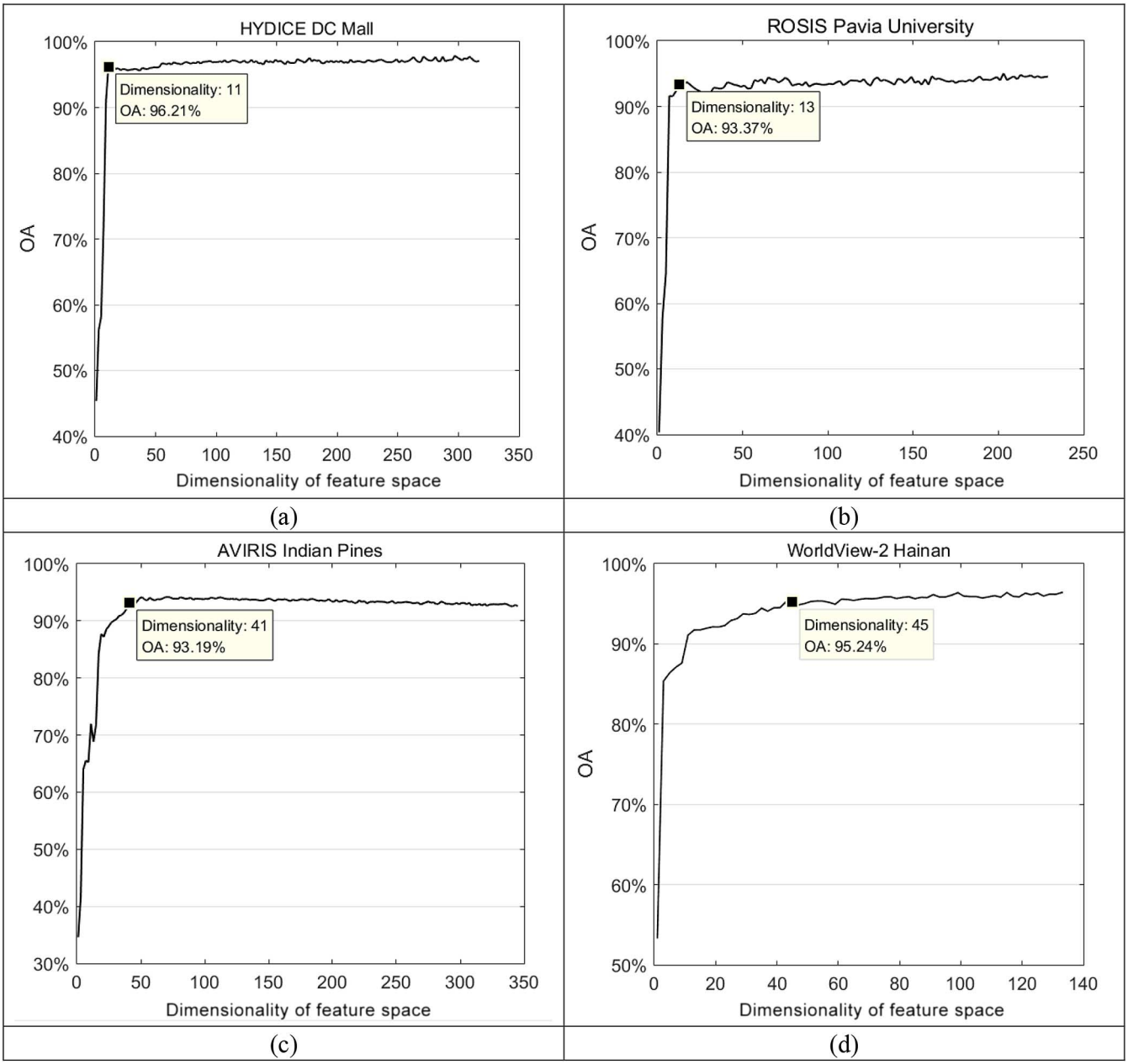

Fig. 14. Relationship between classification accuracy (OA) and the dimensionality of feature space consisting of spectral bands and GDMPs. The so-called turning points (from which accuracy tends to be stable and comparable to the full feature space) are marker in the accuracy curves.

4) Hainan: In this test, a total of 45 features are selected and focused on [Fig. 14(d)]. Thirty six of the 45 selected features are derived from GDMPs, and 32 of the 36 features correspond to the across-scale profiles.

The feature contributions are analyzed in Figs. 13 and 14. The importance of the GDMPs features as well as the spectral signals is computed and ranked based on the Gini index in the RF decision. The number of each feature sources (spectral, DMPs, GDMPs) that are selected at the turning point, first 20-D and first 50-D, is recorded for comparison. Note that the turning point (Fig. 14) indicates where the selected features can achieve a steady classification accuracy that is comparable to the full feature space.

According to the above analysis, we can draw the conclusion that the relevant features from GDMPs play a much more important role than DMPs and spectral signals in the classification task, as they are dominant in the selected feature space in all the test cases. Compared to original DMPs, across-scale DMPs make it possible to obtain the entire differential profiles, depicting the full-shaped spectrum of objects in an image. In addition, through feature selection procedure implemented by RF, a similar classification accuracy can be reached with much less features compared to the high-dimensional hyperspectral and GDMPs feature space.

F. Additional Comparison Between DMPs and GDMPs

In this section, we separated DMPs from GDMPs, and classification was, therefore, conducted on the remaining feature

TABLE X
ACCURACIES (%) OF DMPS, GDMPS–DMPS, AND GDMPS WITH GEODESIC RECONSTRUCTION

Data set	Accuracy (%)	DMPs	GDMPs-DMPs	GDMPs
HYDICE	OA	93.43±1.12	97.32±1.11	97.41±1.21
	AA	96.08±0.45	97.70±0.52	98.26±0.58
	Kappa	92.03±1.35	96.71±1.35	96.82±1.47
ROSIS	OA	86.62±2.40	93.90±1.57	96.22±1.67
	AA	92.18±1.02	96.05±0.52	96.98±0.57
	Kappa	82.87±2.92	92.02±1.95	95.28±2.09
AVIRIS	OA	88.53±1.05	90.70±1.12	92.45±0.73
	AA	90.45±0.77	92.54±0.61	93.89±0.39
	Kappa	86.94±1.19	89.38±1.26	91.43±0.83
WV-2	OA	94.31±0.99	95.00±0.72	96.59±0.69
	AA	94.14±0.68	94.79±0.35	96.41±0.54
	Kappa	93.28±1.23	93.81±0.88	95.98±0.85

sets, called "GDMPs–DMPs." This experiment is to further test whether the proposed GDMPs have better ability for feature representation than the traditional DMPs. The results are reported in Table X. It can be clearly seen that when removing DMPs from GDMPs, the remaining feature set achieved very close accuracy to the GDMPs, and still outperformed the traditional DMPs in all the cases. This phenomenon shows that GDMPs are an effective and meaningful extension to the DMPs, for extracting structural features from MPs.

IV. CONCLUSION

In this study, we propose GDMPs for spatial/structural feature extraction and classification of remote sensing images. Compared to the traditional DMPs, the main superiority of GDMPs is that they can describe across-scale DMPs, which is more appropriate for the multiscale characteristics and complex landscapes of remote sensing image scenes.

Subsequently, in order to address the information redundancy in the GDMPs, RF is used for feature selection and classification.

In this research, the important conclusions drawn from the experimental results are summarized as follows.

1) DMPs and GDMPs can greatly improve the classification results, when compared to spectral-only information, since DMPs and GDMPs can effectively represent the structural information of an image for discriminating between spectrally similar classes.
2) The proposed GDMPs show a better performance in terms of classification accuracy than the original DMPs under circumstances of both geodesic and partial reconstruction. It can be attributed to the ability of the GDMPs to provide scale-span differential profiles, some of which are more informative for the complex geospatial space and more discriminative for the spectral-alike information classes.
3) RF is used to interpret the GDMPs as it is capable of dealing with high-dimensional data with redundant information and evaluating the variable importance according to its "out-of-bag" error. It should be noted that only a few features selected according to feature importance can achieve considerable accuracy of the original feature space.

In summary, it can be concluded that the newly introduced GDMPs can describe more complete structural information of an image and can be a standard technique for feature extraction from remote sensing images. In the future, we plan to discuss the different methods of dimension reduction implemented for the proposed GDMPs and attempt more applications based on GDMPs, such as change detection and object detection.

ACKNOWLEDGMENT

The authors would like to thank Prof. D. A. Landgrebe, Purdue University, USA, for providing the HYDICE data set and Prof. P. Gamba, University of Pavia, Italy, for providing the Pavia University data. They would also like to thank the insightful suggestions from the anonymous reviewers, which significantly improved the quality of this paper.

REFERENCES

[1] S. W. Myint, N. S. N. Lam, and J. M. Tylor, "Wavelets for urban spatial feature discrimination: Comparisons with fractal, spatial autocorrelation, and spatial co-occurrence approaches," *Photogramm. Eng. Remote Sens.*, vol. 70, no. 7, pp. 803–812, Jul. 2004.
[2] X. Huang, L. P. Zhang, and P. X. Li, "An adaptive multiscale information fusion approach for feature extraction and classification of IKONOS multispectral imagery over urban areas," *IEEE Geosci. Remote Sens. Lett.*, vol. 4, no. 4, pp. 654–658, Oct. 2007.
[3] M. Pesaresi, A. Gerhardinger, and F. Kayitakire, "A robust built-up area presence index by anisotropic rotation-invariant textural measure," *IEEE J. Sel. Topics Appl. Earth Observ. Remote Sens.*, vol. 1, no. 3, pp. 180–192, Sep. 2008.
[4] X. Huang, X. B. Liu, and L. P. Zhang, "A multichannel gray level co-occurrence matrix for multi/hyperspectral image texture representation," *Remote Sens.*, vol. 6, no. 9, pp. 8424–8445, Sep. 2014.
[5] S. Geman and D. Geman, "Stochastic relaxation, gibbs distributions, and the bayesian restoration of images," *IEEE Trans. Pattern Anal. Mach. Intell.*, vol. PAMI-6, no. 6, pp. 721–41, Jun. 1984.
[6] C. Zhu and X. Yang, "Study of remote sensing image texture analysis and classification using wavelet," *Int. J. Remote Sens.*, vol. 19, no. 16, pp. 3197–3203, Jan. 1998.
[7] X. Huang and L. P. Zhang, "An SVM ensemble approach combining spectral, structural, and semantic features for the classification of high-resolution remotely sensed imagery," *IEEE Trans. Geosci. Remote Sens.*, vol. 51, no. 1, pp. 257–272, Jan. 2013.
[8] T. Ojala, M. Pietikainen, and T. Maenpaa, "Multiresolution gray-scale and rotation invariant texture classification with local binary patterns," *IEEE Trans. Pattern Anal. Mach. Intell.*, vol. 24, no. 7, pp. 971–987, Jul. 2002.
[9] T. Ahonen, A. Hadid, and M. Pietikainen, "Face description with local binary patterns: Application to face recognition," *IEEE Trans. Pattern Anal. Mach. Intell.*, vol. 28, no. 12, pp. 2037–2041, Dec. 2006.
[10] W. Li, C. Chen, H. J. Su, and Q. Du, "Local binary patterns and extreme learning machine for hyperspectral imagery classification," *IEEE Trans. Geosci. Remote Sens.*, vol. 53, no. 7, pp. 3681–3693, Jul. 2015.
[11] S. D. Newsam and C. Kamath, "Retrieval using texture features in high-resolution multispectral satellite imagery," in *Proc. SPIE Data Min. Knowl. Discovery Theory Tools Technol.*, Apr. 2004, pp. 21–32.
[12] W. Li and Q. Du, "Gabor-filtering-based nearest regularized subspace for hyperspectral image classification," *IEEE J. Sel. Topics Appl. Earth Observ. Remote Sens.*, vol. 7, no. 4, pp. 1012–1022, Apr. 2014.
[13] M. Pesaresi and J. A. Benediktsson, "A new approach for the morphological segmentation of high-resolution satellite imagery," *IEEE Trans. Geosci. Remote Sens.*, vol. 39, no. 2, pp. 309–320, Feb. 2001.
[14] J. A. Benediktsson, M. Pesaresi, and K. Arnason, "Classification and feature extraction for remote sensing images from urban areas based on morphological transformations," *IEEE Trans. Geosci. Remote Sens.*, vol. 41, no. 9, pp. 1940–1949, Sep. 2003.
[15] J. Chanussot, J. A. Benediktsson, and M. Fauvel, "Classification of remote sensing images from urban areas using a fuzzy possibilistic model," *IEEE Geosci. Remote Sens. Lett.*, vol. 3, no. 1, pp. 40–44, Jan. 2006.

[16] X. Huang, L. P. Zhang, and L. Wang, "Evaluation of morphological texture features for mangrove forest mapping and species discrimination using multispectral IKONOS imagery," *IEEE Geosci. Remote Sens. Lett.*, vol. 6, no. 3, pp. 393–397, Jul. 2009.
[17] J. A. Benediktsson, J. A. Palmason, and J. R. Sveinsson, "Classification of hyperspectral data from urban areas based on extended morphological profiles," *IEEE Trans. Geosci. Remote Sens.*, vol. 43, no. 3, pp. 480–491, Mar. 2005.
[18] M. Dalla Mura, J. A. Benediktsson, B. Waske, and L. Bruzzone, "Morphological attribute profiles for the analysis of very high resolution images," *IEEE Trans. Geosci. Remote Sens.*, vol. 48, no. 10, pp. 3747–3762, Oct. 2010.
[19] M. D. Mura, A. Villa, J. A. Benediktsson, J. Chanussot, and L. Bruzzone, "Classification of hyperspectral images by using extended morphological attribute profiles and independent component analysis," *IEEE Geosci. Remote Sens. Lett.*, vol. 8, no. 3, pp. 542–546, May 2011.
[20] P. R. Marpu, M. Pedergnana, M. D. Mura, S. Peeters, J. A. Benediktsson, and L. Bruzzone, "Classification of hyperspectral data using extended attribute profiles based on supervised and unsupervised feature extraction techniques," *Int. J. Image Data Fusion*, vol. 3, no. 3, pp. 269–298, 2012.
[21] X. Huang *et al.*, "Multiple morphological profiles from multicomponent-base images for hyperspectral Image classification," *IEEE J. Sel. Topics Appl. Earth Observ. Remote Sens.*, vol. 7, no. 12, pp. 4653–4669, Dec. 2014.
[22] P. Ghamisi, M. Dalla Mura, and J. A. Benediktsson, "A survey on spectral–spatial classification techniques based on attribute profiles," *IEEE Trans. Geosci. Remote Sens.*, vol. 53, no. 5, pp. 2335–2353, May 2015.
[23] L. Breiman, "Random forests," *Mach. Learn.*, vol. 45, no. 1, pp. 5–32, Oct. 2001.
[24] T. Bylander, "Estimating generalization error on two-class datasets using out-of-bag estimates," *Mach. Learn.*, vol. 48, no. 1–3, pp. 287–297, Jul./Sep. 2002.
[25] J. Serra, *Image Analysis and Mathematical Morphology*. New York, NY, USA: Academic Press, 1983.
[26] R. Bellens, S. Gautama, L. Martinez-Fonte, W. Philips, J. C.-W. Chan, and F. Canters, "Improved classification of VHR images of urban areas using directional morphological profiles," *IEEE Trans. Geosci. Remote Sens.*, vol. 46, no. 10, pp. 2803–2813, Oct. 2008.
[27] W. Z. Liao, R. Bellens, A. Pizurica, W. Philips, and Y. G. Pi, "Classification of hyperspectral data over urban areas using directional morphological profiles and semi-supervised feature extraction," *IEEE J. Sel. Topics Appl. Earth Observ. Remote Sens.*, vol. 5, no. 4, pp. 1177–1190, Aug. 2012.
[28] P. Soille, *Morphological Image Analysis: Principles and Applications*. New York, NY, USA: Springer, 2013.
[29] M. Fauvel, J. A. Benediktsson, J. Chanussot, and J. R. Sveinsson, "Spectral and spatial classification of hyperspectral data using SVMs and morphological profiles," *IEEE Trans. Geosci. Remote Sens.*, vol. 46, no. 11, pp. 3804–3814, Nov. 2008.
[30] L. Breiman, J. Friedman, C. J. Stone, and R. A. Olshen, *Classification and Regression Trees*. Boca Raton, FL, USA: CRC press, 1984.
[31] M. Pal, "Random forest classifier for remote sensing classification," *Int. J. Remote Sens.*, vol. 26, no. 1, pp. 217–222, 2005.
[32] L. Breiman, "RF/tools: A class of two-eyed algorithms." in *Proc. SIAM Workshop*, San Francisco, CA, USA, May. 2003, pp. 1–56.
[33] P. Ghamisi, J. A. Benediktsson, G. Cavallaro, and A. Plaza, "Automatic framework for spectral-spatial classification based on supervised feature extraction and morphological attribute profiles," *IEEE J. Sel. Topics Appl. Earth Observ. Remote Sens.*, vol. 7, no. 6, pp. 2147–2160, Jun. 2014.

Xin Huang (M'13–SM'14) received the Ph.D. degree in photogrammetry and remote sensing from Wuhan University, Wuhan, China, in 2009.

He is with the State Key Laboratory of Information Engineering in Surveying, Mapping, and Remote Sensing (LIESMARS), Wuhan University. He is currently a Full Professor with Wuhan University, where he teaches remote sensing, photogrammetry, image interpretation, etc. He is the Founder and Director of the Institute of Remote Sensing Information Processing (IRSIP), School of Remote Sensing and Information Engineering, Wuhan University. He has authored more than 65 peer-reviewed articles in the international journals. His research interests include hyperspectral data analysis, high-resolution image processing, pattern recognition, and remote sensing applications.

Dr. Huang was the Lead Guest Editor of the special issue on information extraction from high-spatial-resolution optical remotely sensed imagery for the IEEE JOURNAL OF SELECTED TOPICS IN APPLIED EARTH OBSERVATIONS AND REMOTE SENSING (vol. 8, no. 5, May 2015). Since 2014, he serves as an Associate Editor of the IEEE GEOSCIENCE AND REMOTE SENSING LETTERS. He was the recipient of the Top-Ten Academic Star of Wuhan University in 2009, the Boeing Award for the Best Paper in Image Analysis and Interpretation from the American Society for Photogrammetry and Remote Sensing (ASPRS) in 2010, the New Century Excellent Talents in University from the Ministry of Education of China in 2011, the National Excellent Doctoral Dissertation Award of China in 2012, and the China National Science Fund for Excellent Young Scholars in 2015. In 2011, he was recognized by the IEEE Geoscience and Remote Sensing Society (GRSS) as the Best Reviewer of IEEE GEOSCIENCE AND REMOTE SENSING LETTERS. He was the winner of the IEEE GRSS 2014 Data Fusion Contest.

Xiaopeng Han received the B.S degree in surveying engineering from the Central South University, Changsha, China, in 2014. He is currently pursuing the Ph.D. degree in photogrammetry and remote sensing at the State Key Laboratory of Information Engineering in Surveying, Mapping, and Remote Sensing (LIESMARS), Wuhan University, Wuhan, China.

His research interests include high-resolution image processing, information extraction, machine learning, and remote sensing applications.

Liangpei Zhang (M'06–SM'08) received the B.S. degree in physics from Hunan Normal University, Changsha, China, in 1982, the M.S. degree in optics from the Xi'an Institute of Optics and Precision Mechanics, Chinese Academy of Sciences, Xi'an, China, in 1988, and the Ph.D. degree in photogrammetry and remote sensing from Wuhan University, Wuhan, China, in 1998.

He is currently the Head of the Remote Sensing Division, State Key Laboratory of Information Engineering in Surveying, Mapping, and Remote Sensing (LIESMARS), Wuhan University. He is also a "Chang-Jiang Scholar" Chair Professor appointed by the Ministry of Education of China. He is currently a Principal Scientist for the China State Key Basic Research project (2011–2016) appointed by the Ministry of National Science and Technology of China to lead the remote sensing program in China. He has authored more than 450 research papers and 5 books. He is the holder of 15 patents. His research interests include hyperspectral remote sensing, high-resolution remote sensing, image processing, and artificial intelligence.

Dr. Zhang is a Fellow of the Institution of Engineering and Technology (IET), Executive Member (board of governor) of the China National Committee of International Geosphere–biosphere programme, Executive Member of the China Society of Image and Graphics, etc. He regularly serves as a Co-Chair of the series *SPIE Conferences on Multispectral Image Processing and Pattern Recognition*, *Conference on Asia Remote Sensing*, and many other conferences. He is the Founding Chair of the IEEE Geoscience and Remote Sensing Society (GRSS) Wuhan Chapter. He edits several conference proceedings, issues, and geoinformatics symposiums. He also serves as an Associate Editor of the *International Journal of Ambient Computing and Intelligence, International Journal of Image and Graphics, International Journal of Digital Multimedia Broadcasting, Journal of Geo-Spatial Information Science, and Journal of Remote Sensing,* and the Guest Editor of *Journal of Applied Remote Sensing and Journal of Sensors*. He is currently serving as an Associate Editor of the IEEE TRANSACTIONS ON GEOSCIENCE AND REMOTE SENSING. He was the General Chair for the 4th IEEE GRSS WORKSHOP ON HYPERSPECTRAL IMAGE AND SIGNAL PROCESSING: EVOLUTION IN REMOTE SENSING (WHISPERS) and the Guest Editor of JSTARS. He was the recipient of the 2010 Best Paper Boeing Award and the 2013 Best Paper ERDAS Award from the American Society of Photogrammetry and Remote Sensing (ASPRS), the Best Reviewer Awards from IEEE GRSS for his service to the IEEE JOURNAL OF SELECTED TOPICS IN EARTH OBSERVATIONS AND APPLIED REMOTE SENSING (JSTARS) in 2012 and the IEEE GEOSCIENCE AND REMOTE SENSING LETTERS (GRSL) in 2014. His research teams won the top three prizes of the IEEE GRSS 2014 Data Fusion Contest, and his students have been selected as the winners or finalists of the IEEE INTERNATIONAL GEOSCIENCE AND REMOTE SENSING SYMPOSIUM (IGARSS) student paper contest in recent years.

Jianya Gong received the Ph.D. degree in photogrammetry and remote sensing form Wuhan Technical University of Surveying and Mapping, Wuhan, China, in 1992.

He is a Professor with the State Key Laboratory of Information Engineering in Surveying, Mapping, and Remote Sensing (LIESMARS), Wuhan University, Wuhan, China. He is an Academician of the Chinese Academy of Sciences, Beijing, China. His research interests include remote sensing image processing, spatial data infrastructure, geospatial data sharing, and interoperability.

Dr. Gong is the President of Commission VI of the *International Society for Photogrammetry and Remote Sensing*.

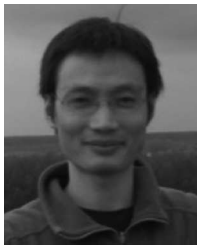

Wenzhi Liao (M'14) received the B.S. degree in mathematics from Hainan Normal University, Haikou, China, in 2006, the Ph.D. degree in engineering from South China University of Technology, Guangzhou, China, in 2012, and the Ph.D. degree in computer science engineering from Ghent University, Ghent, Belgium, in 2012.

Since 2012, he has been a Postdoctoral Researcher with Ghent University. His research interests include pattern recognition, remote sensing, image processing, mathematical morphology, multitask feature learning, multisensor data fusion, and hyperspectral image restoration.

Dr. Liao is a member of the Geoscience and Remote Sensing Society (GRSS) and IEEE GRSS Data Fusion Technical Committee (DFTC). He was the recipient of the "Best Paper Challenge" Awards on both the 2013 IEEE GRSS Data Fusion Contest and the 2014 IEEE GRSS Data Fusion Contest.

Jon Atli Benediktsson (S'84–M'90–SM'99–F'04) received the Cand.Sci. degree in electrical engineering from the University of Iceland, Reykjavik, Iceland, in 1984, and the M.S.E.E. and Ph.D. degrees in electrical engineering from Purdue University, West Lafayette, IN, USA, in 1987 and 1990, respectively.

He is currently Rector and Professor of Electrical and Computer Engineering with the University of Iceland. His research interests include remote sensing, biomedical analysis of signals, pattern recognition, image processing, and signal processing, and he has published extensively in those fields.

Dr. Benediktsson is a Fellow of SPIE. He is a member of the Association of Chartered Engineers in Iceland (VFI), Societas Scinetiarum Islandica, and Tau Beta Pi. He was the 2011–2012 President of the IEEE Geoscience and Remote Sensing Society (GRSS) and has been on the GRSS AdCom since 2000. He was Editor of the IEEE TRANSACTIONS ON GEOSCIENCE AND REMOTE SENSING (TGRS) from 2003 to 2008 and has served as Associate Editor of the TGRS since 1999, the IEEE GEOSCIENCE AND REMOTE SENSING LETTERS since 2003, and the IEEE ACCESS since 2013. He is on the International Editorial Board of the *International Journal of Image and Data Fusion* and was the Chairman of the Steering Committee of IEEE JOURNAL OF SELECTED TOPICS IN APPLIED EARTH OBSERVATIONS AND REMOTE SENSING (JSTARS) 2007–2010. He is a Cofounder of the biomedical start up company Oxymap. He was the recipient of the Stevan J. Kristof Award from Purdue University in 1991 as outstanding graduate student in remote sensing, the Icelandic Research Council's Outstanding Young Researcher Award in 1997, the IEEE Third Millennium Medal in 2000, the yearly research award from the Engineering Research Institute of the University of Iceland in 2006, the Outstanding Service Award from the IEEE Geoscience and Remote Sensing Society in 2007, and the IEEE/VFI Electrical Engineer of the Year Award in 2013. He was a corecipient of the University of Iceland's Technology Innovation Award in 2004, the IEEE TRANSACTIONS ON GEOSCIENCE AND REMOTE SENSING PAPER Award in 2012, and the IEEE GRSS Highest Impact Paper Award in 2013.